THE JOURNAL OF PHYSICAL CHEMISTRY C
A JOURNAL OF THE AMERICAN CHEMICAL SOCIETY

pubs.acs.org/JPCC

Article

Investigating Catalytic Properties Which Influence Dehydration and Oxidative Dehydrogenation in Aerobic Glycerol Oxidation over Pt/TiO_2

Published as part of The Journal of Physical Chemistry virtual special issue "Cynthia Friend Festschrift".

Max Tigwell, Mark Douthwaite,* Louise R. Smith, Nicholas F. Dummer, David J. Morgan, Donald Bethell, Stuart H. Taylor,* and Graham J. Hutchings*

Cite This: *J. Phys. Chem. C* 2022, 126, 15651−15661

Read Online

ACCESS | Metrics & More | Article Recommendations | Supporting Information

ABSTRACT: The use of heterogeneous catalysts to convert glycerol into lactic acid has been extensively investigated in recent years. Several different strategies have been employed, but importantly, the highest production rates of lactic acid are achieved through aerobic oxidation under alkaline conditions. Despite the progress made in this area, insight into how the catalytic properties influence the selectivity of the competing pathways, oxidative dehydrogenation and dehydration, remains limited. Developing a deeper understanding is therefore critical, if process commercialization is to be realized. Using a model Pt/TiO_2 catalyst, we set out to investigate how the supported metal particle size and support phase influenced the selectivity of these two pathways. Both these parameters have a profound effect on the reaction selectivity. Using a range of characterization techniques and through adopting a systematic approach to experimental design, important observations were made. Both pathways are first instigated through the oxidative dehydrogenation of glycerol, leading to the formation of glyceraldehyde or dihydroxyacetone. If these intermediates desorb, they rapidly undergo dehydration through a reaction with the homogeneous base in solution. Based on the experimental evidence we therefore propose that selectivity to lactic acid is influenced by surface residence time.

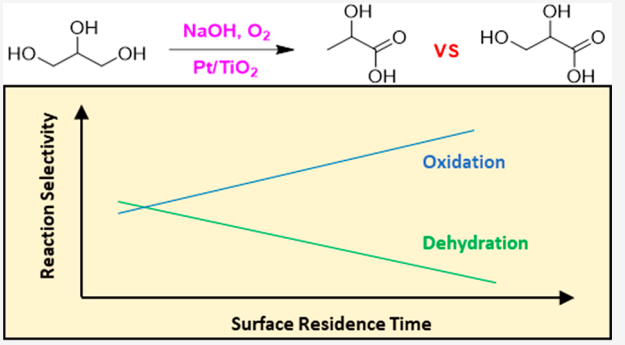

INTRODUCTION

The global demand for biofuels is projected to grow by 28% from 2021 to 2026, with net zero legislation considered to be a key driving force.[1] Biofuels are an attractive alternative to conventional fossil fuels; they are sustainable, as they can be produced directly from biomass. Biodiesel is one of the more common biofuels available and is produced commercially through the transesterification of fatty acids. This is a well-established process, but it has its limitations as approximately 10 wt % of glycerol is produced as a byproduct.[2] Glycerol is, however, a highly functionalized molecule which can be valorized into a variety of different compounds,[3,4] but significant investment into the development of these processes is required if these concepts are to be realized commercially.

Lactic acid (LA) is a high-value chemical, which can be produced from the selective oxidation of glycerol.[5] It has many applications in the food, pharmaceutical, and cosmetic industries, but perhaps most pertinently, it is used as a monomer for the production of polylactide (PLA).[6−8] According to a report by market research, the market size of polylactic acid was valued at $566 million in 2021 and is expected to advance at a compound annual growth rate of over 26.6% from 2022 to 2030.[9] The ever-growing demand could be attributed to regulations imposed by the EU which banned the use of single-use plastics in 2021.[10] Packaging has the largest revenue share accounting for 36% in 2022, due to the productions of bottles, containers, and fresh food packaging.[9]

A key challenge associated with the selective oxidation of glycerol to lactic acid is that many different products can be formed (Scheme 1). Most examples of glycerol oxidation over supported metal catalysts involve reaction under alkaline aqueous conditions. The presence of base is important, as it significantly promotes the activation of glycerol.[11,12] This has been attributed to a change in the way the C−H bond is activated,[13,14] which is rate limiting.[15] Interestingly, the morphology of Pt particles has been demonstrated to

Received: May 28, 2022
Revised: August 25, 2022
Published: September 13, 2022

Scheme 1. Glycerol Oxidation to Various Products under Aerobic, Alkaline Conditions[a]

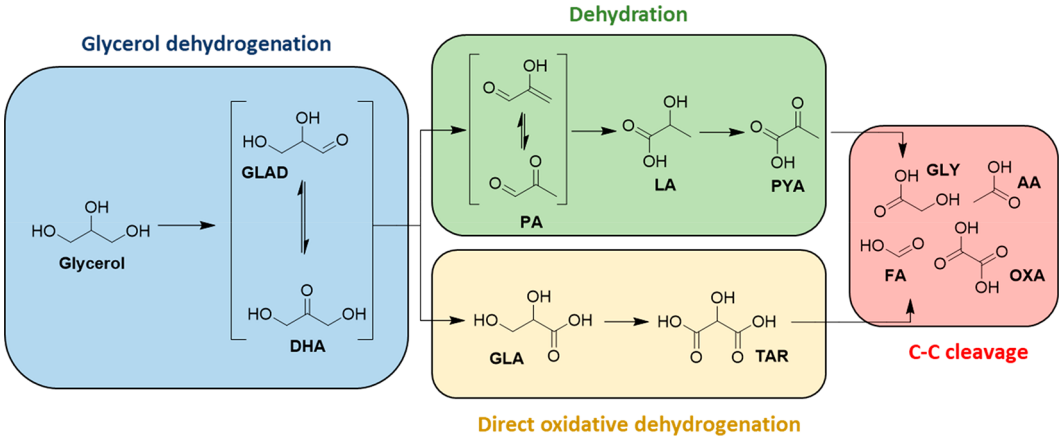

[a]Key: glyceraldehyde (GLAD); dihydroxyacetone (DHA); pyruvaldehyde (PA); lactic acid (LA); pyruvic acid (PYA); glyceric acid (GLA); tartronic acid (TAR); glycolic acid (GLY); acetic acid (AA); formic acid (FA); oxalic acid (OXA).

dramatically influence the rate of glycerol oxidation but only marginally influenced the reaction selectivity,[16] thus, reducing the approaches that researchers can adopt to control selectivity in this reaction.

In the selective oxidation of glycerol, there are two competing pathways: oxidative dehydrogenation (ODH) and dehydration (Scheme 1). Current understanding of the reaction profile suggests that glycerol first undergoes ODH to either glyceraldehyde (GLAD) or dihydroxyacetone (DHA). Statistically, this should yield a GLAD/DHA ratio of 2:1, but the structure and properties of the catalyst will likely influence which alcohol moiety is activated. This equilibrium is also considered to be dynamic; thus, it is highly influenced by reaction conditions such as pH.[17,18] Next, these intermediates can either undergo a sequential ODH to glyceric acid (GLA) and subsequently tartronic acid (TAR), or they can undergo dehydration to pyruvaldehyde (PA). In the presence of base, PA rapidly rearranges through a 1,2-hydride shift to produce LA.[19] Additional downstream products can also be produced, either through further oxidation or through C−C cleavage. C−C cleavage reactions are particularly undesirable, as they lead to the formation of C_1 and C_2 products. These cleavages are proposed to occur through reactions between C_3 intermediates and H_2O_2 (produced *in situ*).[20]

Given the variety of products which can form, it is unsurprising that the reaction conditions can dramatically influence product selectivity. Using a model $AuPt/TiO_2$ catalyst, Evans et al.[19] demonstrated that increasing the pH and reaction temperature could significantly increase reaction selectivity to LA, by promoting the dehydration reaction. No such dependence was observed with oxygen pressure, which can be explained by the fact that the role of O_2 in such reactions is to remove electrons from the catalyst surface.[15,21,22] However, increasing oxygen pressure was demonstrated to increase C−C scission. To counteract this, other groups have developed methods to convert glycerol into LA under anaerobic conditions.[23] Here, transfer dehydrogenation of glycerol is achieved using an unsaturated hydrogen acceptor, such as levulinic acid, benzene, and cylcohexene. After this step, the product (GLAD or DHA) reacts with homogeneous base to produce LA. This is an interesting strategy; by switching off the C−C cleavage and ODH pathways, an exceptionally high reaction selectivity to LA is achievable.

A number of studies have also demonstrated that LA can be produced under base-free conditions.[20,22,24] In such examples, the dehydration of GLAD or DHA to PA and its subsequent rearrangement to LA is catalyzed by Bronsted and/or Lewis acid sites.[25] Conducting this in the absence of base is extremely advantageous from an industrial perspective, as it eliminates complications downstream which could arise from the presence of inorganic additives. Nevertheless, from a process perspective, productivity is also a critical consideration. The rate of glycerol conversion and LA productivity from reactions conducted under: (i) aerobic basic conditions, (ii) aerobic base-free conditions, and (iii) anaerobic conditions in the presence of a hydrogen acceptor are compared in Table S1. It is clear from these data that each process has its merits. Nevertheless, from an activity perspective, aerobic reactions conducted in the presence of base seem to be most advantageous.

It is well-known that the reaction conditions,[19] the choice of supported metal or support,[12,26] can influence LA selectivity under alkaline, aerobic conditions. Despite the significant amount of work conducted in this area,[3,27] to the best of our knowledge, no systematic study investigating how particle size and electronic effects influence reaction selectivity has been conducted. We therefore considered this to be an important line of enquiry and based our study around a model 1 wt % Pt/TiO_2 catalyst, which was selected due to the fact that the high performance of this catalyst is already well established in the literature.[22,28−30]

METHODS

Materials. Acetic acid (Fisher Scientific, ≥99%); ammonium hydroxide (Acros Organics, 85% in H_2O); chloroplatinic acid (Johnson Matthey, Assay 30.53%); dihydroxyacetone (Chem Cruz, ≥99%); glyceraldehyde (Chem Cruz, ≥99%); glyceric acid (Sigma-Aldrich, ≥99%); glycerol (Alfa Aesar, ≥99.5+%); glycolic acid (Sigma-Aldrich, ≥99%); hydrochloric acid (Fisher Scientific, 37 wt %); isopropyl alcohol (Fisher Scientific); DL-lactic acid (Alfa Aesar, 1.0 N standardized); oxalic acid (Sigma-Aldrich, ≥99%); phosphoric acid (Sigma-Aldrich, 85 wt % in H_2O, ≥99.99%); poly(vinyl alcohol) (Sigma-Aldrich, MW 9,000−10,000, 80% hydrolyzed); sodium borohydride (Sigma-Aldrich, ≥99.9%); sodium hydroxide (Fisher Scientific); sodium pyruvate (Sigma-Aldrich, ≥99%);

https://doi.org/10.1021/acs.jpcc.2c03680
J. Phys. Chem. C 2022, 126, 15651−15661

sulfuric acid (Fisher Scientific, ≥95%); tartronic acid (Fluka, ≥97%); titanium tetraisopropoxide (Sigma-Aldrich, ≥98%); water (Fisher Scientific, HPLC grade).

Material Synthesis. *Synthesis of Titanium Dioxide.* The following sol−gel procedure was used for the synthesis of TiO_2 precursors in this study. Titanium tetraisopropoxide (TTIP) was added to isopropyl alcohol (200 mL) and acidified to pH 2 using concentrated HCl (37 wt %). To this solution, NH_4OH (2M) was added dropwise until pH 9 was reached. The slurry was stirred for a further hour, over which time, the pH was maintained at pH 9. Finally, the resulting precipitate was separated from the liquid medium through centrifugation, washed with H_2O and dried in an oven at 110 °C for 16 h. The resultant precursor was then calcined in a tube furnace (static air) at temperatures between 500−700 °C (ramp rate = 10 °C/min). The nomenclature used to describe these materials is TiO_2-X (where X = calcination temperature).

Synthesis of Pt/TiO_2 Catalysts by Sol-Immobilization. The following procedure was used to synthesize 1 g batches of the Pt supported catalysts used in this study. NOTE: All the TiO_2 supported catalysts had a theoretical Pt loading of 1 wt %. H_2PtCl_6 (0.59 mL, 8.41 g/L) was added to a beaker containing H_2O (400 mL) under stirring. To this, poly(vinyl alcohol) solution (0.65 mL, 1 wt % in water) was added and stirred for 15 min. $NaBH_4$ (1.911 mL, 7.57 g/L) was then added to the solution, which was left to stir for a further 30 min. The colloidal Pt nanoparticles were then immobilized through the addition of TiO_2 (0.99 g) and the solution was acidified to pH 2 through the dropwise addition of conc. H_2SO_4. After 1 h of additional stirring, the slurry was filtered in air using a Buchner setup and the catalyst was washed with deionized water (800 mL). The catalyst was then dried in an oven at 110 °C for 16 h.

Synthesis of 1 wt % Pt−Y/TiO_2-600 Materials. To understand how the Pt particle size influenced catalyst performance in the aerobic oxidation of glycerol under alkaline conditions, an additional series of catalysts were synthesized where calcination treatments were used to increase the Pt particle size. For this, portions of the Pt/TiO_2-600 catalyst were taken and calcined (static air) at specific temperatures (200−500 °C). The nomenclature used to describe these materials is Pt−Y/TiO_2-600 (where Y = the calcination temperature used). After these calcinations, each of the catalysts were thermally reduced (250 °C) under flowing 5% H_2/Ar (5 mL min^{-1}) for 3 h.

Catalyst Testing. All catalyst performance experiments were conducted in a 50 mL glass Colaver reactor. This is glass single neck reactor, which comprises an inlet to connect directly to a gas regulator. A photograph of a typical reaction setup in a glass Colaver reactor is provided in Figure S1. These experiments were conducted under a range of conditions, which are outlined in the associated Figure/Table captions. A typical experimental procedure is outlined below:

The desired quantity of catalyst (typically 29.0 mg) was added to the glass reactor, followed by aqueous glycerol (10 mL of a 0.6 M) and NaOH solutions (10 mL, 2.4 M) and a magnetic stirrer bar. The reaction vessel was purged five times under stirring with pressurized O_2 (3 bar) and placed in the preheated oil bath (typically 110 °C). The reaction vessel was stirred at 1000 rpm for the stated reaction time. After completion, the reactor vessel was cooled on ice to room temperature and depressurized, and the resulting reaction mixture was filtered. The reaction samples were diluted 10-fold in H_2O and analyzed by high performance liquid chromatography (HPLC). Quantification of the postreaction effluent was conducted using an Agilent 1260 Infinity HPLC fitted with refractive index and diode array detectors. The reactants and products were separated using a Metacarb 67 h column. The eluent was aqueous H_3PO_4 (0.01 M), and the mobile phase flow rate was set to 0.25 mL min^{-1}. Products and reactants were identified through comparison to a range of standards. The quantification of reactants and products was determined using an external calibration method.

In some cases, the substrate (and its concentration) and/or the pH of the solution was changed. For these experiments, identical experimental procedures were used to the ones above—only the identity of the substrate or the concentration of the substrate or base was changed.

Catalyst Characterization. *Powder X-ray Diffraction.* XRD was used to assess the phase purity and crystallite size of each TiO_2 material. Analysis was conducted on a (θ−θ) PANalytical X'pert Pro powder diffractometer system fitted with a CuKα X-ray source run at 40 kV and 40 mA. An X'Celerator detector was used to measure scattered X-rays. Each sample was scanned from 2θ = 10° to 80°. Diffraction patterns of phases were identified through reference to standards from the International Center for Diffraction Data (ICDD) database.

X-ray Photoelectron Spectroscopy. XPS measurements were performed using a ThermoFisher Scientific K-Alpha$^+$ photoelectrons spectrometer utilizing a microfocused monochromatic Al Kα source ($h\nu$ = 1486.6 eV) operating at 72 W (6 mA × 12 kV). Charge compensation was achieved using a combination of low energy electrons and argon ions. Calibration to the C 1s line for adventitious carbon was found be unreliable giving a variance of at least 0.5 eV between samples, therefore all XPS data has been calibrated to the Ti $2p_{3/2}$ core-level, taken to be 458.8 eV. High-resolution and survey scans were performed at energies of 40 and 150 eV, respectively. Data were analyzed using CasaXPS (v2.3.24PR1.0) using modified Scofield sensitivity factors and an electron escape dependence according to the TPP-2 M equation.

BET analysis was conducted on a Quantachrome Quadrosorb instrument; the samples were first degassed at 200 °C for 4 h. Once degassed, 25-point nitrogen adsorption isotherms were collected at −196 °C, and data were analyzed using the BET method.

Transmission Electron Microscopy. TEM was carried out with a Jeol 2100 with a LAB6 filament operating at 200 kV. Each sample was prepared by dispersing the powdered catalyst in ethanol and dropping the suspension onto a lacey carbon film over a 300-mesh copper grid.

In Situ CO Diffuse Reflectance Infrared Fourier Transform Spectroscopy. DRIFTS experiments were carried out using a Bruker Tensor 27 FTIR spectrometer with a liquid N_2 cooled MCT detector. The spectra were recorded with 4 cm^{-1} resolution with 32 scans per spectrum. The catalysts were pretreated with N_2 for 30 min to remove any surface absorbates. Then CO (2% CO/He) was passed over the catalyst scanning every minute for 20 min to achieve saturation. Finally, the system was purged with N_2 to remove any gas phase CO.

In Situ 1,2-propanediol. DRIFTS experiments were carried out using a Bruker Tensor 27 FTIR spectrometer with a liquid N_2 cooled MCT detector. The spectra were recorded with 4

https://doi.org/10.1021/acs.jpcc.2c03680
J. Phys. Chem. C 2022, 126, 15651−15661

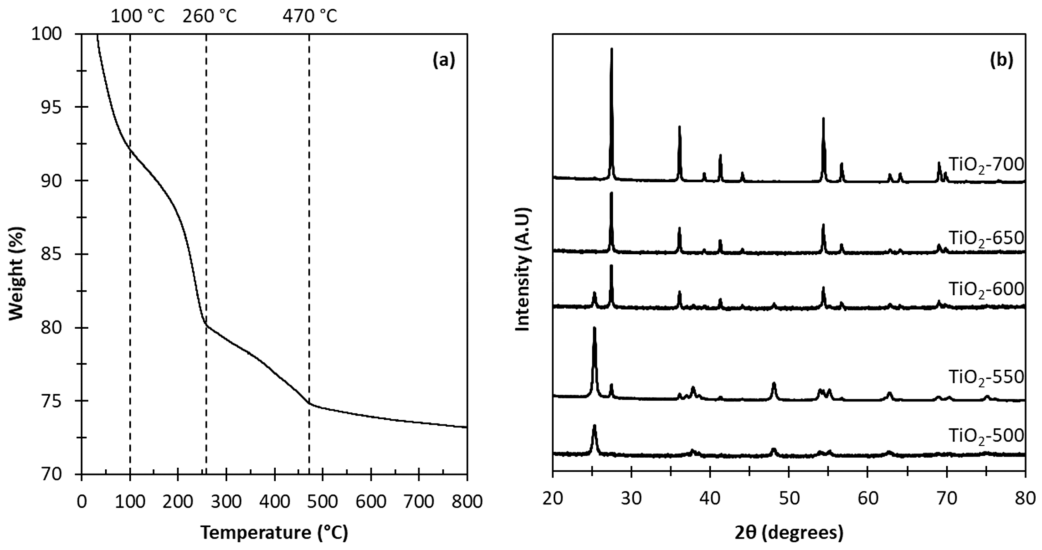

Figure 1. (a) Thermogravimetric analysis of the TiO_2 precursor under aerobic conditions. (b) XRD patterns of the TiO_2 precursor after calcination at 500, 550, 600, 650, and 700 °C.

Table 1. Influence of the Calcination Temperature on the Structural and Textural Properties of the Synthesized TiO_2 Materials

Material ID	Anatase[a] /%	Rutile[a]/%	Lattice strain/%	Surface Area[b]/ m^2 g^{-1}	Pore Volume[b]/cm^3 g^{-1}	Ave. Pore Size[c]/nm
TiO_2-700	0	100	0.226	13	0.025	1.53
TiO_2-650	0	100	0.226	13	0.039	1.53
TiO_2-600	32	68	0.149	28	0.075	1.79
TiO_2-550	90	10	0.102	30	0.096	1.69
TiO_2-500	100	0	0.246	41	0.104	1.90

[a]Proportions of anatase and rutile estimated using Rietveld Refinement. [b]Surface area from N_2 adsorption isotherms using a five-point BET method. [c]Pore volume and average pore size estimated from the desorption isotherms, in accordance with the BJH method.

cm^{-1} resolution with 32 scans per spectrum. The catalysts were pretreated with N_2 (30 mL min^{-1}) at 110 °C for 1 h to remove any surface absorbates. After 1 h, a flow of N_2 (30 mL min^{-1}) was passed through a bubbler heated at 60 °C containing 1,2 propanediol before being passed over the catalyst. The spectra were collected in the range of 4000−400 cm^{-1} with a scan every minute for 1 h. After which, the bubbler was switched off and N_2 was allowed to flow over the catalyst to remove any physisorbed 1,2 propanediol. Repeated spectra were collected over a further 30 min.

The number of exposed Pt surface sites was estimated using the geometric Mackay icosahedral model.[31] Using this method, it was possible to estimate the number of Pt sites associated with the exposed particle surface and the entire particle volume. Using the equation $d = (2n + 1) \times 0.272$ (nm), where n is the number of shells in the Mackay model, the particle diameter (d) could be acquired. Then, the total number of atoms in a particle (N) could be acquired using the equation $N_{tot} = {}^{10}/_{3}n^3 + 5n^2 + {}^{11}/_{3}n + 1$ and the total number of exposed surface sites (N_{surf}) could be estimated using the equation $N_{surf} = 10n^2 + 2$. These data were used to calculate the glycerol turnover frequency (TOF) and lactic acid productivity for each of the catalysts used in this study. The active Pt surface area was determined with CO pulse chemisorption analysis using a Micromeritics Autochem 2920 instrument equipped with a TCD detector. The catalysts were pretreated under N_2/Ar (100 °C, 10/min, 30 min), and the gas flow was switched to Ar for a further 30 min, after which, the vessel was allowed to cool to room temperature. After pretreatment, the CO chemisorption analysis was carried out using 1% CO/He at 35 °C. The catalysts were completely saturated after 10 pulses. For analysis of the results, a coordination of one CO molecule to an active Pt site is assumed. Due to the presence of PVA stabilizer on the metal nanoparticles, active site quantification from the CO chemisorption experiments was deemed to be unreliable in this study.

RESULTS AND DISCUSSION

It is well established that strong metal−support interactions (SMSI) in supported heterogeneous materials can have a dramatic influence on their performance as catalysts.[32,33] These enhancements can be induced either through morphological and/or electronic modifications. TiO_2 supported Pt catalysts are particularly prone to SMSI effects. Lewera et al.[34] previously demonstrated that the addition of an intermediary TiO_2 layer to a Pt/C catalyst (forming Pt/TiO_2/C) led to increased electron density in the supported Pt particles. This was, in turn, correlated to the catalysts increased oxygen reduction activity. As electronic metal support interactions can be strongly influenced by the support properties, it was pertinent to consider how the TiO_2 phase might influence performance in this reaction.

To investigate this, a large batch of TiO_2 precursor was synthesized using a base-catalyzed sol−gel method. Thermal gravimetric analysis (TGA) was subsequently used to examine the decomposition profile of the precursor under aerobic conditions (Figure 1a). The initial mass loss at 30 °C−100 °C, was attributed to the removal of chemically and physically bound H_2O.[35] The second notable mass loss, from 100 to 260 °C, was assigned to the emission of H_2O from the dehydration

https://doi.org/10.1021/acs.jpcc.2c03680
J. Phys. Chem. C 2022, 126, 15651−15661

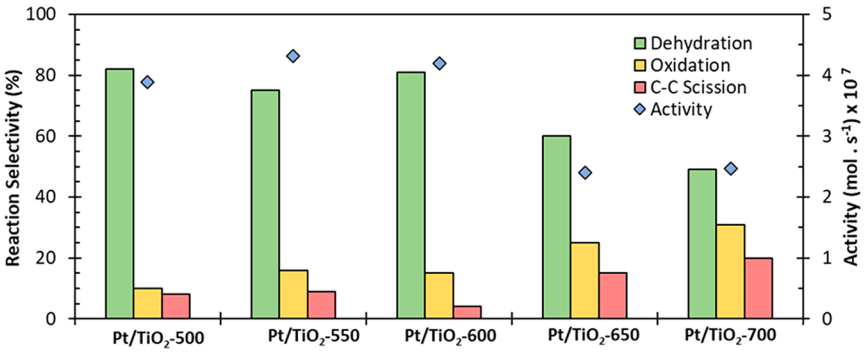

Figure 2. Influence of the support calcination temperature (550−700 °C) on glycerol conversion activity and reaction selectivity to dehydration, oxidation, and C−C cleavage products. *Reaction conditions*: Reaction volume (20 mL); glycerol concentration (0.3 M); sodium hydroxide concentration (1.2 M); O_2 pressure (3 bar); temperature (110 °C); catalyst (0.029 g).

of H_4TiO_4 to TiO_2.[36] The final mass loss event, at 260−470 °C, could be attributed to the decomposition of residual unhydrolyzed alkoxy groups bound to titanium.[36] Based on these observations, aliquots of the TiO_2 precursor were calcined at varying temperatures above this threshold (500, 550, 600, 650, and 700 °C). Each of these materials were subsequently probed by XRD to identify how the calcination temperature influenced the TiO_2 phase (Figure 1b).

The XRD patterns from these experiments are presented in Figure 1b and were compared to standards for anatase (ICDD 01-086-1157) and rutile (ICDD 01-089-0555). Evidently, the calcination temperature had a significant impact on the phase composition of the TiO_2. After calcination at 500 °C, anatase was the dominant polymorph. This is unsurprising given that anatase possesses a lower surface energy than rutile. As the calcination temperature was increased, the proportion of rutile present also increased.[37] Saalinraj and co-workers observed a similar trend and concluded that the higher thermal stability of rutile phase is the driving force for this phase transformation.[38] Rietveld refinement was subsequently used to quantify the proportion of both polymorphs in these materials (Table 1). This was conducted through analysis of the full anatase and rutile reflections. After calcination to 650 °C there was no evidence of any anatase reflections, suggesting that the majority (if not all) of the anatase had been converted into rutile. Next, the textural properties of the TiO_2 materials were probed by N_2 physisorption (Table 1). A clear decrease in the specific surface area of TiO_2 is observed as the calcination temperature was increased, which correlates with the apparent increase in the anatase and rutile crystallite sizes. This is also consistent with the observed decrease in pore diameter and pore volume, as the calcination temperature was increased.

The series of TiO_2 materials were subsequently employed as supports for Pt nanoparticles. PVA-stabilized Pt colloids were generated using an established method,[39] and deposited onto each of the TiO_2 materials (theoretical Pt wt % = 1). The nomenclature used to describe each of these materials was Pt/TiO_2-X (where X = calcination temperature in °C). A colloidal method was selected for the preparation of the TiO_2 supported Pt catalysts as it is highly effective at controlling the particle size of the active metal components.[40] This is important, as it is well established that particle size can dramatically influence a supported metal catalysts ability to oxidize alcohols aerobically.[41,42] Thus, reducing (or eliminating) particle size variability across samples would make it easier to draw correlations between the support properties and catalyst performance. To assess whether this strategy had been effective, the Pt particle size of each catalyst was probed by TEM. Representative micrographs and particle size histograms for each of the catalysts are presented in Figure S2. The mean Pt particle sizes were determined to be consistent (3.15−3.26 nm) except for the Pt/TiO_2-600 catalyst, which possessed a significantly smaller mean particle size (2.27 nm). With the exception of the latter catalyst, the colloidal preparation strategy had indeed been effective; the fractional exposure of Pt was not influenced by textural or structural properties of the supports.

Each of the TiO_2 supported Pt catalysts were subsequently tested for the aerobic oxidation of glycerol under alkaline conditions. Catalytic performance was assessed at low conversion (<30%), as it is considered important to compare activity when other factors (such as substrate availability) were not influential. For simplicity, reaction products were separated into three groups (Scheme 1): oxidation products, dehydration products, and C−C cleavage products. The summarized results from these experiments are presented in Figure 2, but full product distributions are also listed in Table S2. It should be noted that control experiments conducted over the Pt/TiO_2-500 catalyst confirmed that the catalytic reactions were unlikely to be limited by solid/liquid or O_2/liquid mass transfer (Figure S3).

The rate of glycerol conversion decreased slightly as the calcination temperature was increased. The one notable outlier was the Pt-TiO_2-600 catalyst, which possessed a notably smaller mean Pt particle size (Figure S1). Perhaps more interesting, is the notable decrease in selectivity to dehydration products, as the calcination temperature of the support was increased. This decrease in selectivity to dehydration products was evidently a result of increased selectivity to oxidation and C−C cleavage products. This suggests that C−C cleavage must predominantly arise from oxidation products (GLA or TA). Ultimately, what these data demonstrate is that the phase of the TiO_2 does indeed influence catalyst performance in this reaction which, from the microscopy data (Figure S2), cannot be attributed to the fraction of exposed Pt sites.

To investigate why these catalysts performed differently in the reaction, the series of catalysts were probed by XPS and CO-DRIFTS. Previously, Yang et al.[43] proposed that the electron density in TiO_2 supported Pt particles significantly influenced their performance in the oxidation of 1-octanol. The XPS Pt*4f* region for each of the catalysts is presented in Figure 3(a). The Pt present in all of the catalysts was fully reduced as

https://doi.org/10.1021/acs.jpcc.2c03680
J. Phys. Chem. C 2022, 126, 15651−15661

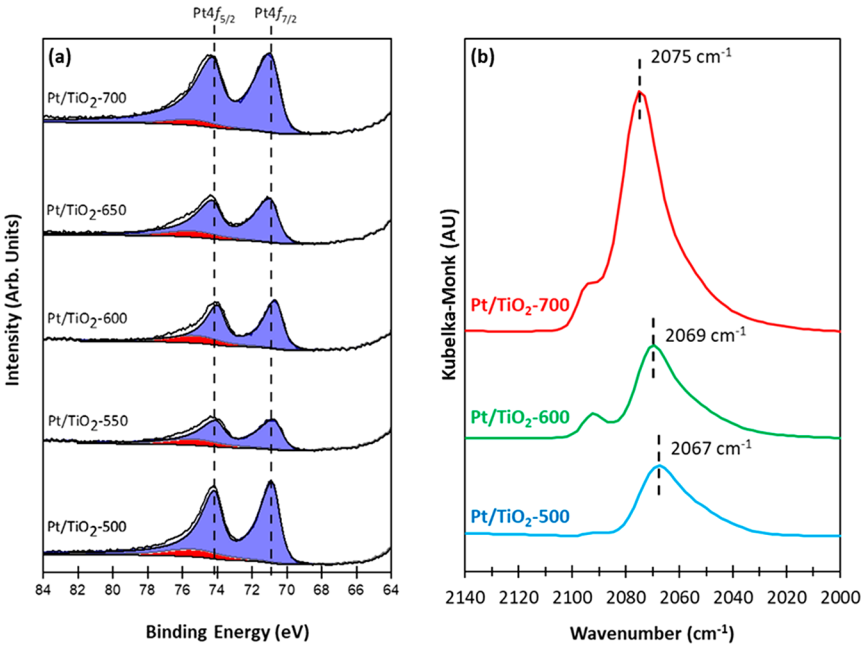

Figure 3. Influence of support calcination temperature on electronic properties of the Pt components. (a) XPS was used to probe the Pt4*f* region. The blue colored peaks correspond to a single Pt^0 state, and the red colored peak corresponds to a TiO_2 loss structure. (b) *In situ* CO-DRIFTS spectra are displayed.

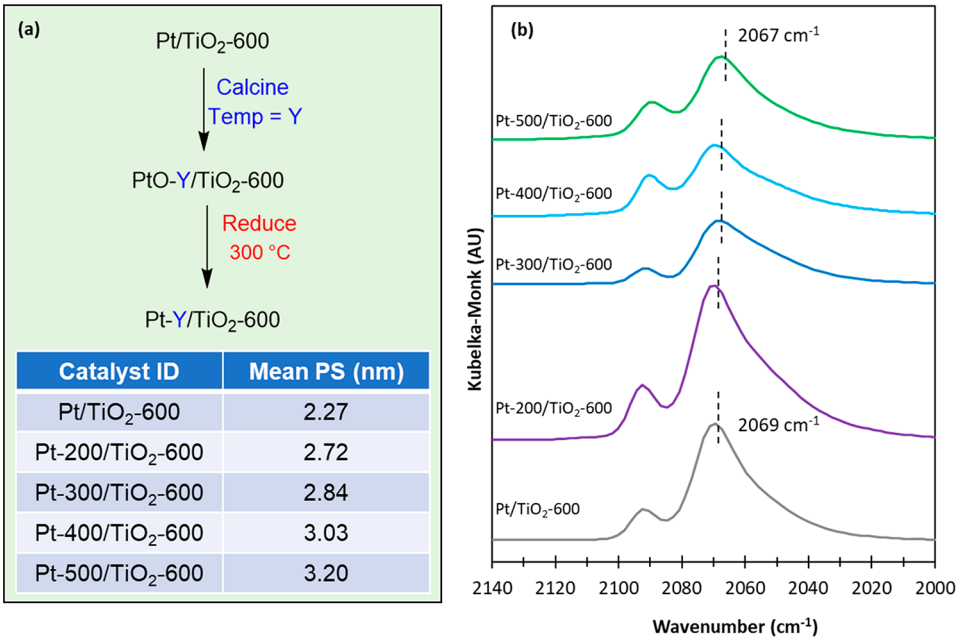

Catalyst ID	Mean PS (nm)
Pt/TiO_2-600	2.27
Pt-200/TiO_2-600	2.72
Pt-300/TiO_2-600	2.84
Pt-400/TiO_2-600	3.03
Pt-500/TiO_2-600	3.20

Figure 4. (a) Schematic representation of catalyst synthesis procedure. Nomenclature and mean Pt particle size (PS) for each of the catalysts. (b) *In situ* CO-DRIFTS spectra of each catalyst.

evidenced by the asymmetric peak shapes of the Pt4*f* signals. The Pt4$f_{7/2}$ binding energies recorded at 70.6 eV are all below that of bulk Pt (measured as 71.1 eV on a Pt foil), but subtly increase to 71 eV with increasing calcination temperature of the support. Typically the binding energy of metal nanoparticles is expected to be at a higher binding energy;[44] however, the observed values herein are clearly below that of bulk Pt, suggesting an enhanced electron density. Analogous *in situ* CO-DRIFTS experiments also yielded some interesting information (Figure 3(b). Each of the catalysts exhibited absorption bands which are characteristic of linear CO adsorption on Pt nanoparticles.[45−47] Notably, two peaks indicative of linear CO-Pt vibrations on metallic Pt nanoparticles were observed in the spectra. This phenomenon is commonly observed in CO-DRIFTS experiments over supported Pt catalysts and is typically attributed to the adsorption of CO onto different energy Pt sites. The high energy peak is characteristic of the CO-Pt bond vibration on flat Pt sites, while the lower energy peak can be ascribed to CO-Pt vibrations on Pt edge/corner sites.[46] These two peaks cannot be attributed to CO adsorbed on cationic Pt sites or gas phase CO, whose characteristic bond vibrations are typically

https://doi.org/10.1021/acs.jpcc.2c03680
J. Phys. Chem. C 2022, 126, 15651−15661

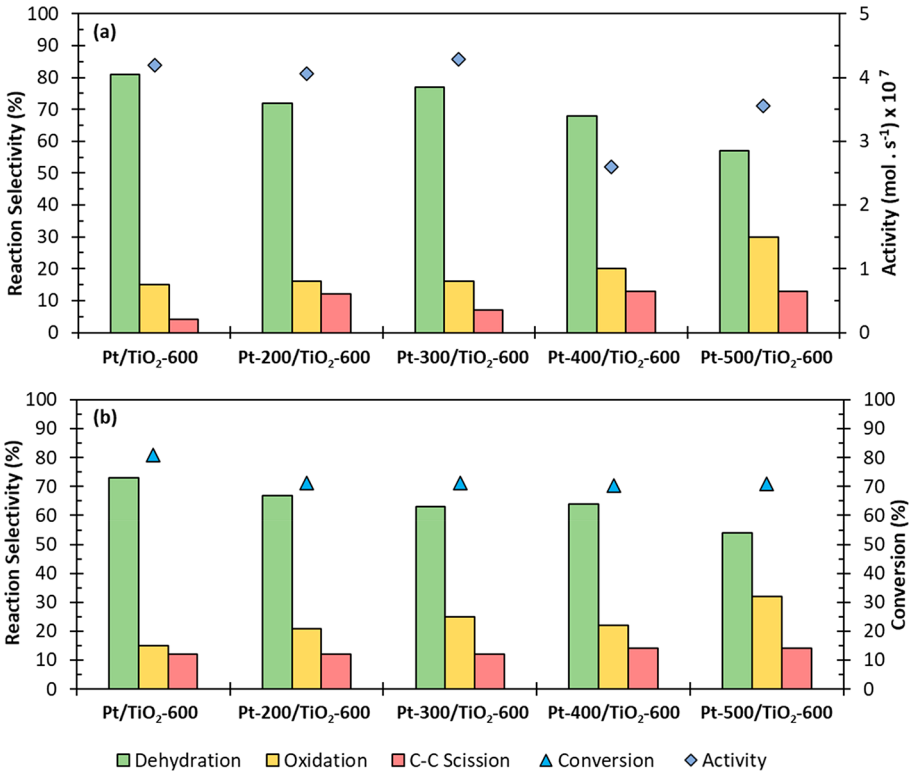

Figure 5. Influence of the Pt particle size for Pt/TiO_2-600 catalysts on activity and reaction selectivity at (a) low conversion (<30% glycerol converted) and (b) high conversion. *Reaction conditions*: Reaction volume (20 mL); glycerol concentration (0.3 M); sodium hydroxide concentration (1.2 M); O_2 pressure (3 bar); temperature (110 °C); catalyst (0.029 g).

observed at much higher energies (>2100 cm^{-1}). Interestingly, the energy of this vibration appeared to increase as the calcination temperature of the support was increased. Increases in vibration bond energies in such catalysts have previously been attributed to decreases in bond length,[48] which, in turn, can be indicative of increased electron density in the particle. If this is indeed the case here, then it could suggest that substrate binding energy might influence the reaction selectivity.

Given that metal particle size can influence electronic properties,[48] it seemed logical to assess whether the Pt particle size, in the Pt/TiO_2 catalysts, could also influence selectivity. As we have already demonstrated that the phase of the support can influence reactivity, it was important to develop a method to probe this without changing the composition of the support. To do this, portions of the Pt/TiO_2-600 catalyst, which possessed the smallest mean Pt particle size, were taken and recalcined at a variety of different temperatures (200, 300, 400, and 500 °C). 500 °C was selected as the highest temperature to thermally treat these catalysts, as it was thought that exceeding this might lead to structural changes in the TiO_2 support (having already been calcined at 600 °C). The nomenclature used to describe these catalysts is Pt−Y/TiO_2-600, where Y is the temperature used to calcine the Pt/TiO_2-600 catalyst. Given that Pt^0 nanoparticles can readily oxidize when subjected to aerobic thermal treatments, each of the materials were subsequently thermally reduced under a flow of $5\%H_2/Ar$ at 250 °C. A schematic representation of this procedure is presented in Figure 4a. To ensure that this had been successful and to ensure that the additional thermal treatments had not influenced the structure of the TiO_2 support, each catalyst was subjected to further characterization by XPS and XRD. Analysis of the Pt*4f* region confirmed that only reduced Pt was present in each of the materials (Figure S4). XRD also confirmed that the distribution of anatase and rutile in each of the catalysts was consistent (Figure S5). To establish whether the additional thermal treatments had successfully increased the Pt particle size, each of the materials was probed by TEM. Representative micrographs and particle size distributions for each of these catalysts are presented in Figure S6. The mean particle size of the Pt particles was determined to increase consistently, from 2.27 to 3.20 nm (Figure 4(a)).

Next, this series of Pt−Y/TiO_2-600 catalysts were assessed for the aerobic oxidation of glycerol at both low and high conversion (Figure 5 panels (a) and (b), respectively). Once again, for simplicity, the selectivity data presented in Figure 5 is separated into the three primary product groupings; full product distributions for the reactions conducted at low and high conversion are presented in Tables S3 and S4, respectively. The initial rates of glycerol consumption generally decreased as the Pt particle size increased. More interestingly, selectivity to dehydration products was decreased, again at the expense of selectivity to both oxidation and C−C cleavage products. This suggests that the Pt particle size can also influence the oxidation and dehydration selectivity in this reaction.

To assess whether this might also be a result of changes to the electronic properties of the supported particles, the series of catalysts were once again subjected to *in situ* CO-DRIFTS experiments (Figure 4(b)). All of the catalysts exhibited vibrational bands indicative of linear CO adsorption on Pt nanoparticles. Rather surprisingly, only a minor red shift of *ca.* 2 cm^{-1} was observed across the series of catalysts, as the calcination temperature was increased. This is contradictory to

https://doi.org/10.1021/acs.jpcc.2c03680
J. Phys. Chem. C 2022, 126, 15651−15661

Table 2. Influence of pH on Glyceraldehyde and Dihydroxyacetone Conversion in the Presence and Absence of the Pt/TiO_2-600 Catalyst[a]

				Selectivity										
pH	Cat.	Sub.	Con. (%)	DHA	GLAD	LA	OXA	TAR	GLA	GLY	PYA	FA	AA	CMB (%)
14	NO	GLAD	100.0	0.0		80.1	0.5	1.0	2.1	0.0	0.7	9.9	5.8	60.8
13	NO	GLAD	100.0	32.4		45.6	0.0	3.4	11.7	0.0	0.2	5.3	1.4	50.7
11.5	NO	GLAD	70.0	100.0		0.0	0.0	0.0	0.0	0.0	0.0	0.0	0.0	87.3
10	NO	GLAD	<1	0.0		0.0	0.0	0.0	0.0	0.0	0.0	0.0	0.0	100.8
7	YES	GLAD	34.7	0.0		0.0	0.0	0.0	100.0	0.0	0.0	0.0	0.0	100.4
14	YES	DHA	100		0.0	78.2	0.0	0.0	0.0	0.0	0.0	5.6	7.9	98.2
14	NO	DHA	100		0.0	79.4	0.0	0.0	0.0	0.0	0.0	5.1	8.4	100.5
11.5	NO	DHA	<1		0.0	0.0	0.0	0.0	0.0	0.0	0.0	0.0	0.0	101.2
10	NO	DHA	<1		0.0	0.0	0.0	0.0	0.0	0.0	0.0	0.0	0.0	99.7
7	YES	DHA	<1		0.0	0.0	0.0	0.0	0.0	0.0	0.0	0.0	0.0	100.2

[a]Reaction Conditions: Reaction solution (20 mL, 0.1 M dihydroxyacetone or glyceraldehyde, varied NaOH concentration); 3 bar O2; 110 °C; Pt/TiO_2-600 (0.029g, if present). Key: Con. (Conversion); GLAD (Glyceraldehyde); DHA (Dihydroxyacetone); LA (Lactic Acid); OXA (Ocalic Acid); TAR (Tartronic Acid); GLA (Glyceric Acid); GLY (Glycolic Acid); PYA (Pyruvic Acid); FA (Formic Acid); AA (Acetic Acid); CMB (Carbon Mass Balance).

the larger blue shift observed with the previous set of catalysts, which correlated with decreased dehydration selectivity. Given that only a very small change in the bond energy was observed, it is unlikely that the different reaction selectivity exhibited by the Pt−Y/TiO_2-600 catalysts are a result of changes to the electronic properties of the Pt nanoparticles. As such, its logical to consider that reaction selectivity exhibited by this set of catalysts might be governed by another factor.

It is widely accepted that glycerol oxidation is initiated through a heterogeneously catalyzed oxidative dehydrogenation step, which leads to the formation of either DHA (via secondary alcohol oxidation) or GLAD (via primary alcohol oxidation). Given that these compounds exist in equilibrium[18] it is surprising that under alkaline conditions, these intermediates are never observed. Evans et al.[19] demonstrated that, under comparable conditions to those used in this study, DHA and GLAD are rapidly consumed. Building on this understanding, we conducted additional reactions from GLAD and DHA at different pH (Table 2). In both cases, the pH of the aqueous medium had a significant effect on substrate conversion, in the absence of a heterogeneous catalyst. In the reactions from GLAD there was no conversion observed at pH 10, while at pH 11.5 only DHA was observed. Increasing the concentration of $^-$OH further to pH 13 and pH 14 resulted in increasing quantities of LA. The base catalyzed interconversion of aldehydes into ketones is well-established in carbohydrate chemistry; known to proceed through the Lobry de Bruyn-Van Ekenstein transformation. These observations are supported by the reactions conducted from DHA; no GLAD was observed in any of the reactions. The higher carbon mass balance observed in the reactions from DHA indicate that a base promoted bimolecular condensation is also likely to occur from GLAD. While it is clear from Table 2 that DHA is favored at elevated pH, it does not necessarily suggest that dehydration proceeds from this intermediate, as GLAD dehydration is far more likely and can proceed readily via a E1cB mechanism. Thus, when sufficient hydroxyl concentration is present, GLAD is likely to undergo dehydration and supplemental DHA will be converted back to GLAD to rebalance the equilibrium. This process will be rapid and is not likely to influence the overall kinetics.

From this enhanced understanding, the influence the support phase (Figure 2 and Table S2) and Pt particle size (Figure 5 and Tables S3 and S4) has on the reaction selectivity can be considered. Given the extremely high pH used in these reactions (*ca.* pH 14), it is likely that any GLAD present immediately undergoes dehydration upon desorption from the catalyst surface after alcohol dehydrogenation. The resultant product, pyruvaldehyde, will also rapidly rearrange to LA. As these steps are catalyzed homogeneously, and are therefore likely to be very fast, it is unlikely that a notable quantity of GLAD will re-adsorb and undergo further oxidative dehydrogenation to oxidation products. As such, it is logical to suggest that all the direct oxidation products observed are probably formed through a multiple surface transformation process from glycerol (dehydrogenation, followed by hydration and subsequent dehydrogenation), in one adsorption cycle (Scheme 2).

We must then consider how the physicochemical properties of the support and Pt particle size are likely to influence this. Rutile-rich TiO_2 supports were determined to decrease the CO-Pt bond length, which was tentatively ascribed to

Scheme 2. Under Highly Basic Conditions, Desorbed Glyceraldehyde or Dihydroxyacetone Is More Likely to Undergo Base Catalyzed Dehydration than Re-Adsorb and Undergo Further Oxidative Dehydrogenation to Glyceric Acid[a]

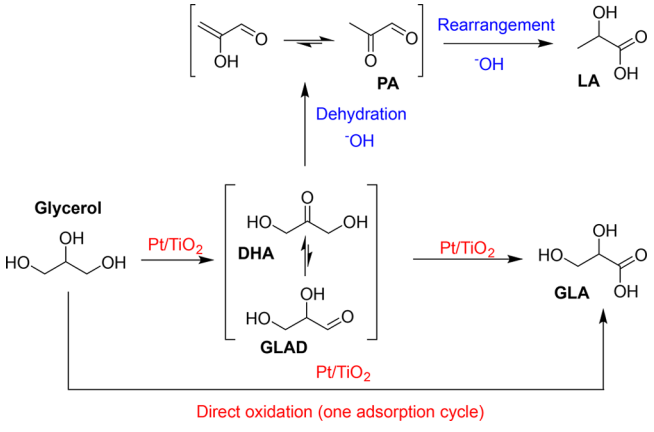

[a]KEY: dihydroxyacetone (DHA); glyceraldehyde (GLAD); pyruvaldehyde (PA); lactic acid (LA); glyceric acid (GLA).

https://doi.org/10.1021/acs.jpcc.2c03680
J. Phys. Chem. C 2022, 126, 15651−15661

increased electron density in the Pt nanoparticles. If this is indeed the case, it could explain why higher selectivity to oxidation products is observed over these catalysts. Increased substrate binding energy could favor a two-step surface oxidation process or promote the readsorption of GLAD prior to its rearrangement to DHA. Given that no significant differences in electronic properties were observed for the Pt–Y/TiO_2 catalysts, it is likely that another explanation exists for the changeable selectivity observed with these catalysts. As selectivity to oxidation products increases with an increasing Pt particle size, it is plausible to suggest that the bonding mode of glycerol is responsible. As glycerol is a triol, it can form surface alkoxides at three different positions. Thus, surface geometry permitting, glycerol could form a bidentate alkoxy intermediate. Subsequently in situ FTIR and DRIFTS experiments, using glycerol and 1,2-propanediol as probe molecules, were conducted to try and validate our hypothesis. Unfortunately, no supplemental evidence could be acquired from these experiments. The data acquired from in situ FTIR experiments was limited by spectral saturation from physisorbed probe molecule and/or water. On the contrary, the data acquired from in situ DRIFTS experiments was limited by poor resolution. The poor resolution was attributed to a lack of probe molecule adsorption, owing to its extremely low vapor pressure. Thus, further work is still required to confirm whether surface residence time is indeed a mitigating factor that influences selectivity in this reaction.

Given that the experimental approaches used to validate our hypothesis failed, the use of DFT to investigate this theoretically is a logical next step. Zaffran et al.[49] established that Bronsted–Evans–Polanyi relationships for C–H and O–H bond cleavages, when surface mediated alcohols were hydrogen-bonded to chemisorbed water, was an effective method of predicting how glycerol dehydrogenation proceeds over a Pt surface. The authors deduced that, over a Pt surface, enol formation was most favored. It is however worth noting that the authors determined that corresponding barriers to DHA and GLAD were not much higher. More recently, Valter et al.[50] demonstrated that $*CH_2OH$ and CH_3O* species were effective descriptors for glycerol dehydrogenation over a broad variety of metals (Ru, Co, Rh, Ir, Ni, Pd, Pt, Cu, Aq, and Au). The authors demonstrated that the binding energies of these descriptors influenced primary vs secondary alcohol dehydrogenation and the resultant adsorption mode of the intermediate. Stronger binding energies for these descriptors resulted in the formation of bidentate intermediates, bonding either through two alkoxy moieties or through one alkoxy and one carboxy moieties. On the contrary, the authors noted that physisorbed DHA was favored by weak binding energies of both descriptors. This particular example provides compelling evidence for the hypothesis provided herein; the substrate binding energy and bonding mode influence selectivity. However, both these examples do not include ^-OH in their calculations. Given that ^-OH greatly influences both glycerol dehydrogenation rate and product selectivity,[30] it is important that similar theoretical measurements are conducted which include ^-OH in the local environment.

The increased TiO_2 and Pt interface sites, which would increase with increased Pt dispersion, is another possible explanation as to why selectivity is influenced by Pt particle size in the Pt–Y/TiO_2-600 catalysts. This is particularly pertinent, given that Zhang et al.[42] determined that Pt particle size had very little influence on lactic acid selectivity over Pt/AC catalysts prepared by deposition precipitation. Given that Bronsted acid and Lewis acid sites in TiO_2 are known to promote dehydration and rearrangement steps in this reaction under base free conditions,[20,51] it is possible that the TiO_2 is also important here. This is particularly pertinent, given the preceding discussion on how binding energy may influence selectivity and the fact that there was no evidence to suggest that the Pt particle size influences CO-Pt bond lengths over these catalysts (Figure 4b).

To assess whether the LA productivity correlated to surface residence time, the number of exposed Pt sites present in each of the catalysts was estimated using the geometric Mackay Icosahedral model.[31] Details relating to this methodology can be found in the experimental section and in Table S5. Based on the number of exposed Pt sites, it was possible to estimate the glycerol TOF and LA productivity for each of the catalysts used in this study (Table S5). Evidently, there is a clear correlation between these two data sets (Figure 6). This suggests that the rate of glycerol consumed is intrinsically linked to the rate in which lactic acid is produced and suggests that surface residence time influences selectivity in this reaction; the shorter is the surface residence time, the higher is the rate of lactic acid produced.

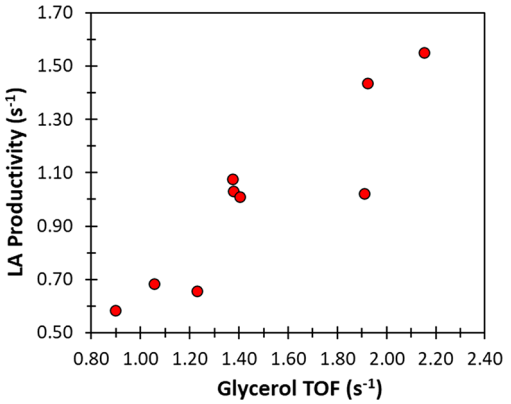

Figure 6. Glycerol TOF is related to the lactic acid productivity observed in the aerobic oxidation of glycerol under aqueous alkaline conditions. The data used to construct this plot are derived from initial rate reactions (0.5 h) conducted over all the catalysts used in this study.

The factors which influence this remain to be hypothetical at this stage. Further work is required, ideally with a supplemental theoretical calculation, to establish whether the substrate binding mode and/or binding energy influences surface residence time. In its current form, this research highlights how notable enhancements in reaction selectivity can be achieved in the aerobic alkaline oxidation of glycerol through tuning the catalyst properties. Based on these suggestions, the development and utilization of a catalyst which can selectively oxidize primary alcohols to aldehydes under aerobic conditions could be highly selective to lactic acid.

CONCLUSIONS

Reaction selectivity in the aerobic oxidation of glycerol over Pt/TiO_2 can be significantly affected by the phase of the support and the Pt particle size. We propose that the phase of the TiO_2 support influences the electronic properties of the supported Pt particles, which influences substrate binding energy. On the contrary, we propose that the Pt particle size

https://doi.org/10.1021/acs.jpcc.2c03680
J. Phys. Chem. C 2022, 126, 15651−15661

influences selectivity through changing the absorption mode of the substrate. Surface residence time appears to be a critical factor which influences selectivity in this reaction, but further evidence is required to establish whether this is attributed to substrate binding energy or adsorption mode. Nevertheless, these data highlight that notable changes to reaction selectivity in this reaction can be achieved through simple tuning of the physicochemical properties of the Pt/TiO_2 catalyst. These new insights into the factors which influence selectivity in this reaction provide new opportunities for the development of even more effective catalysts for this process.

■ ASSOCIATED CONTENT

Supporting Information

The Supporting Information is available free of charge at https://pubs.acs.org/doi/10.1021/acs.jpcc.2c03680.

Additional catalyst testing and characterization data (PDF)

■ AUTHOR INFORMATION

Corresponding Authors

Mark Douthwaite − *Max Planck-Cardiff Centre on the Fundamentals of Heterogeneous Catalysis FUNCAT, Cardiff Catalysis Institute, School of Chemistry, Cardiff University, Cardiff CF10 3AT, United Kingdom*; Email: douthwaitejm@cardiff.ac.uk

Stuart H. Taylor − *Max Planck-Cardiff Centre on the Fundamentals of Heterogeneous Catalysis FUNCAT, Cardiff Catalysis Institute, School of Chemistry, Cardiff University, Cardiff CF10 3AT, United Kingdom*; orcid.org/0000-0002-1933-4874; Email: taylorsh@cardiff.ac.uk

Graham J. Hutchings − *Max Planck-Cardiff Centre on the Fundamentals of Heterogeneous Catalysis FUNCAT, Cardiff Catalysis Institute, School of Chemistry, Cardiff University, Cardiff CF10 3AT, United Kingdom*; orcid.org/0000-0001-8885-1560; Email: hutch@cardiff.ac.uk

Authors

Max Tigwell − *Max Planck-Cardiff Centre on the Fundamentals of Heterogeneous Catalysis FUNCAT, Cardiff Catalysis Institute, School of Chemistry, Cardiff University, Cardiff CF10 3AT, United Kingdom*

Louise R. Smith − *Max Planck-Cardiff Centre on the Fundamentals of Heterogeneous Catalysis FUNCAT, Cardiff Catalysis Institute, School of Chemistry, Cardiff University, Cardiff CF10 3AT, United Kingdom*

Nicholas F. Dummer − *Max Planck-Cardiff Centre on the Fundamentals of Heterogeneous Catalysis FUNCAT, Cardiff Catalysis Institute, School of Chemistry, Cardiff University, Cardiff CF10 3AT, United Kingdom*; orcid.org/0000-0002-0946-6304

David J. Morgan − *Max Planck-Cardiff Centre on the Fundamentals of Heterogeneous Catalysis FUNCAT, Cardiff Catalysis Institute, School of Chemistry, Cardiff University, Cardiff CF10 3AT, United Kingdom*; orcid.org/0000-0002-6571-5731

Donald Bethell − *Max Planck-Cardiff Centre on the Fundamentals of Heterogeneous Catalysis FUNCAT, Cardiff Catalysis Institute, School of Chemistry, Cardiff University, Cardiff CF10 3AT, United Kingdom*

Complete contact information is available at: https://pubs.acs.org/10.1021/acs.jpcc.2c03680

Notes

The authors declare no competing financial interest.

■ ACKNOWLEDGMENTS

The authors would like to acknowledge the CCI-Electron Microscopy Facility which has been funded in part by the European Regional Development Fund through the Welsh Government and the Wolfson Foundation.

■ REFERENCES

(1) IEA. Renewables 2021. *Int. Energy Agency Publ. Int.* 2021, 167.

(2) Demirbas, A. Biofuels Sources, Biofuel Policy, Biofuel Economy and Global Biofuel Projections. *Energy Convers. Manag.* **2008**, *49* (8), 2106−2116.

(3) Checa, M.; Nogales-Delgado, S.; Montes, V.; Encinar, J. M. Recent Advances in Glycerol Catalytic Valorization: A Review. *Catalysts* **2020**, *10* (11), 1−41.

(4) Behr, A.; Eilting, J.; Irawadi, K.; Leschinski, J.; Lindner, F. Improved Utilisation of Renewable Resources: New Important Derivatives of Glycerol. *Green Chem.* **2008**, *10* (1), 13−30.

(5) Razali, N.; Abdullah, A. Z. Production of Lactic Acid from Glycerol via Chemical Conversion Using Solid Catalyst: A Review. *Appl. Catal. A Gen.* **2017**, *543* (12), 234−246.

(6) Pawar, R. P.; Tekale, S. U.; Shisodia, S. U.; Totre, J. T.; Domb, A. J. Biomedical Applications of Poly(Lactic Acid). *Rec. Pat. Regen. Med.* **2014**, *4* (1), 40−51.

(7) Avérous, L. Polylactic Acid: Synthesis, Properties and Applications. *Monomers, Polymers and Composites from Renewable Resources* **2008**, 433−450.

(8) Tyler, B.; Gullotti, D.; Mangraviti, A.; Utsuki, T.; Brem, H. Polylactic Acid (PLA) Controlled Delivery Carriers for Biomedical Applications. *Adv. Drug Delivery Rev.* **2016**, *107*, 163−175.

(9) *Polylactic Acid Market Size, Share And Trends Analysis Report By End Use (Packaging, Agriculture, Transport, Electronics, Textile, Others), By Region, And Segment Forecasts, 2022−2030*; GrandViewResearch, 2022.

(10) *Turning the Tide on Single-Use Plastics*; European Commision Directorate-General for Environment, 2021.

(11) Mallat, T.; Baiker, A. Oxidation of Alcohols with Molecular Oxygen on Platinum Metal Catalysts in Aqueous Solutions. *Catal. Today* **1994**, *19* (2), 247−283.

(12) Carrettin, S.; McMorn, P.; Johnston, P.; Griffin, K.; Kiely, C. J.; Hutchings, G. J. Oxidation of Glycerol Using Supported Pt, Pd and Au Catalysts. *Phys. Chem. Chem. Phys.* **2003**, *5* (6), 1329−1336.

(13) Ide, M. S.; Davis, R. J. The Important Role of Hydroxyl on Oxidation Catalysis by Gold Nanoparticles. *Acc. Chem. Res.* **2014**, *47* (3), 825−833.

(14) Fristrup, P.; Johansen, L. B.; Christensen, C. H. Mechanistic Investigation of the Gold-Catalyzed Aerobic Oxidation of Alcohols. *Catal. Lett.* **2008**, *120* (3−4), 184−190.

(15) Zope, B. N.; Hibbitts, D. D.; Neurock, M.; Davis, R. J. Reactivity of the Gold/Water Interface during Selective Oxidation Catalysis. *Science (80-.).* **2010**, *330* (6000), 74−78.

(16) Zhou, J.; Hu, J.; Zhang, X.; Li, J.; Jiang, K.; Liu, Y.; Zhao, G.; Wang, X.; Chu, H. Facet Effect of Pt Nanocrystals on Catalytical Properties toward Glycerol Oxidation Reaction. *J. Catal.* **2020**, *381*, 434−442.

(17) A. Yaylayan, V.; Harty-Majors, S.; A. Ismail, A. Investigation of DL-Glyceraldehyde-Dihydroxyacetone Interconversion by FTIR Spectroscopy. *Carbohydr. Res.* **1999**, *318* (1−4), 20−25.

(18) Nagorski, R. W.; Richard, J. P. Mechanistic Imperatives for Aldose - Ketose Isomerization in Water: Specific, General Base- and Metal Ion-Catalyzed Isomerization of Glyceraldehyde with Proton and Hydride Transfer. *J. Am. Chem. Soc.* **2001**, *123* (5), 794−802.

(19) Evans, C. D.; Douthwaite, M.; Carter, J. H.; Pattisson, S.; Kondrat, S. A.; Bethell, D.; Knight, D. W.; Taylor, S. H.; Hutchings, G. J. Enhancing the Understanding of the Glycerol to Lactic Acid

Reaction Mechanism over AuPt/TiO $_2$ under Alkaline Conditions. *J. Chem. Phys.* **2020**, *152* (13), 134705.
(20) Cho, H. J.; Chang, C. C.; Fan, W. Base Free, One-Pot Synthesis of Lactic Acid from Glycerol Using a Bifunctional Pt/Sn-MFI Catalyst. *Green Chem.* **2014**, *16* (7), 3428−3433.
(21) Huang, X.; Akdim, O.; Douthwaite, M.; Wang, K.; Zhao, L.; Lewis, R. J.; Pattisson, S.; Daniel, I. T.; Miedziak, P. J.; Shaw, G.; Morgan, D. J.; Althahban, S. M.; Davies, T. E.; He, Q.; Wang, F.; Fu, J.; Bethell, D.; McIntosh, S.; Kiely, C. J.; Hutchings, G. J. Au-Pd Separation Enhances Bimetallic Catalysis of Alcohol Oxidation. *Nature* **2022**, *603* (7900), 271−275.
(22) Douthwaite, M.; Powell, N.; Taylor, A.; Ford, G.; López, J. M.; Solsona, B.; Yang, N.; Sanahuja-Parejo, O.; He, Q.; Morgan, D. J.; Garcia, T.; Taylor, S. H. Glycerol Selective Oxidation to Lactic Acid over AuPt Nanoparticles; Enhancing Reaction Selectivity and Understanding by Support Modification. *ChemCatChem.* **2020**, *12* (11), 3097−3107.
(23) Tang, Z.; Cao, H.; Tao, Y.; Heeres, H. J.; Pescarmona, P. P. Transfer Hydrogenation from Glycerol over a Ni-Co/CeO2 Catalyst: A Highly Efficient and Sustainable Route to Produce Lactic Acid. *Appl. Catal. B Environ.* **2020**, *263* (10), 118273.
(24) Feng, S.; Takahashi, K.; Miura, H.; Shishido, T. One-Pot Synthesis of Lactic Acid from Glycerol over a Pt/L-Nb2O5 Catalyst under Base-Free Conditions. *Fuel Process. Technol.* **2020**, *197* (9), 106202.
(25) De Clippel, F.; Dusselier, M.; Van Rompaey, R.; Vanelderen, P.; Dijkmans, J.; Makshina, E.; Giebeler, L.; Oswald, S.; Baron, G. V.; Denayer, J. F. M.; Pescarmona, P. P.; Jacobs, P. A.; Sels, B. F. Fast and Selective Sugar Conversion to Alkyl Lactate and Lactic Acid with Bifunctional Carbon-Silica Catalysts. *J. Am. Chem. Soc.* **2012**, *134* (24), 10089−10101.
(26) Ftouni, J.; Villandier, N.; Auneau, F.; Besson, M.; Djakovitch, L.; Pinel, C. From Glycerol to Lactic Acid under Inert Conditions in the Presence of Platinum-Based Catalysts: The Influence of Support. *Catal. Today* **2015**, *257*, 267−273.
(27) Zhou, C. H.; Zhao, H.; Tong, D. S.; Wu, L. M.; Yu, W. H. Recent Advances in Catalytic Conversion of Glycerol. *Catal. Rev. - Sci. Eng.* **2013**, *55* (4), 369−453.
(28) Shen, Y.; Zhang, S.; Li, H.; Ren, Y.; Liu, H. Efficient Synthesis of Lactic Acid by Aerobic Oxidation of Glycerol on Au-Pt/TiO2 Catalysts. *Chem. - A Eur. J.* **2010**, *16* (25), 7368−7371.
(29) Komanoya, T.; Suzuki, A.; Nakajima, K.; Kitano, M.; Kamata, K.; Hara, M. A Combined Catalyst of Pt Nanoparticles and TiO2 with Water-Tolerant Lewis Acid Sites for One-Pot Conversion of Glycerol to Lactic Acid. *ChemCatChem.* **2016**, *8* (6), 1094−1099.
(30) Evans, C. D.; Douthwaite, M.; Carter, J. H.; Pattisson, S.; Kondrat, S. A.; Bethell, D.; Knight, D. W.; Taylor, S. H.; Hutchings, G. J. Enhancing the Understanding of the Glycerol to Lactic Acid Reaction Mechanism over AuPt/TiO2 under Alkaline Conditions. *J. Chem. Phys.* **2020**, *152* (13), 134705.
(31) Mackay, A. L. A Dense Non-Crystallographic Packing of Equal Spheres. *Acta Crystallogr.* **1962**, *15* (9), 916−918.
(32) Pan, C. J.; Tsai, M. C.; Su, W. N.; Rick, J.; Akalework, N. G.; Agegnehu, A. K.; Cheng, S. Y.; Hwang, B. J. Tuning/Exploiting Strong Metal-Support Interaction (SMSI) in Heterogeneous Catalysis. *J. Taiwan Inst. Chem. Eng.* **2017**, *74*, 154−186.
(33) Spencer, M. S. Models of Strong Metal-Support Interaction (SMSI) in Pt on TiO2 Catalysts. *J. Catal.* **1985**, *93* (2), 216−223.
(34) Lewera, A.; Timperman, L.; Roguska, A.; Alonso-Vante, N. Metal-Support Interactions between Nanosized Pt and Metal Oxides (WO 3 and TiO2) Studied Using X-Ray Photoelectron Spectroscopy. *J. Phys. Chem. C* **2011**, *115* (41), 20153−20159.
(35) Mueller, R.; Kammler, H. K.; Wegner, K.; Pratsinis, S. E. OH Surface Density of SiO2 and TiO2 by Thermogravimetric Analysis. *Langmuir* **2003**, *19* (1), 160−165.
(36) Wang, J.; Yu, J.; Zhu, X.; Kong, X. Z. Preparation of Hollow TiO2 Nanoparticles through TiO2 Deposition on Polystyrene Latex Particles and Characterizations of Their Structure and Photocatalytic Activity. *Nanoscale Res. Lett.* **2012**, *7*, 646 DOI: 10.1186/1556-276X-7-646.
(37) Wetchakun, N.; Incessungvorn, B.; Wetchakun, K.; Phanichphant, S. Influence of Calcination Temperature on Anatase to Rutile Phase Transformation in TiO 2 Nanoparticles Synthesized by the Modified Sol-Gel Method. *Mater. Lett.* **2012**, *82*, 195−198.
(38) Saalinraj, S.; Ajithprasad, K. C. Effect of Calcination Temperature on Non-Linear Absorption Co-Efficient of Nano Sized Titanium Dioxide (TiO2) Synthesised by Sol-Gel Method. *Mater. Today Proc.* **2017**, *4* (2), 4372−4379.
(39) Cherni, D.; Moussa, N.; Nsib, M. F.; Evangelisti, C.; Prati, L.; Villa, A. Base-Free Glycerol Oxidation over N-TiO2 Supported Au-Pt Catalysts. *React. Kinet. Mech. Catal.* **2019**, *128* (2), 979−990.
(40) Villa, A.; Jouve, A.; Sanchez Trujillo, F. J.; Motta, D.; Prati, L.; Dimitratos, N. Exploring the Effect of Au/Pt Ratio on Glycerol Oxidation in Presence and Absence of a Base. Exploring the Effect of Au/Pt Ratio on Glycerol Oxidation in Presence and Absence of a Base. *Catalyst* **2018**, *8* (2), 54 DOI: 10.3390/catal8020054.
(41) Wang, H.; Gu, X. K.; Zheng, X.; Pan, H.; Zhu, J.; Chen, S.; Cao, L.; Li, W. X.; Lu, J. Disentangling the Size-Dependent Geometric and Electronic Effects of Palladium Nanocatalysts beyond Selectivity. *Sci. Adv.* **2019**, *5* (1), 1−9.
(42) Zhang, C.; Wang, T.; Ding, Y. Influence of Pt Particle Size on the Activity of Pt/AC Catalyst in Selective Oxidation of Glycerol to Lactic Acid. *Catal. Lett.* **2017**, *147* (5), 1197−1203.
(43) Yang, P.; Douthwaite, M.; Pan, J.; Zheng, L.; Hong, S.; Morgan, D. J.; Gao, M.; Li, D.; Feng, J.; Hutchings, G. J. Coordinately Unsaturated O2c-Ti5c-O2csites Promote the Reactivity of Pt/TiO2catalysts in the Solvent-Free Oxidation Ofn-Octanol. *Catal. Sci. Technol.* **2021**, *11* (14), 4898−4910.
(44) Mason, M. G. Electronic Structure of Supported Small Metal Clusters. *Phys. Rev. B* **1983**, *27* (2), 748−762.
(45) Olsen, C. W.; Masel, R. I. An Infrared Study of CO Adsorption on Pt(111). *Surf. Sci.* **1988**, *201* (3), 444−460.
(46) Lentz, C.; Jand, S. P.; Melke, J.; Roth, C.; Kaghazchi, P. DRIFTS Study of CO Adsorption on Pt Nanoparticles Supported by DFT Calculations. *J. Mol. Catal. A Chem.* **2017**, *426*, 1−9.
(47) Allian, A. D.; Takanabe, K.; Fujdala, K. L.; Hao, X.; Truex, T. J.; Cai, J.; Buda, C.; Neurock, M.; Iglesia, E. Chemisorption of CO and Mechanism of CO Oxidation on Supported Platinum Nanoclusters. *J. Am. Chem. Soc.* **2011**, *133* (12), 4498−4517.
(48) Al-Shareef, R.; Harb, M.; Saih, Y.; Ould-Chikh, S.; Anjum, D. H.; Candy, J. P.; Basset, J. M. Precise Control of Pt Particle Size for Surface Structure-Reaction Activity Relationship. *J. Phys. Chem. C* **2018**, *122* (41), 23451−23459.
(49) Zaffran, J.; Michel, C.; Delbecq, F.; Sautet, P. Towards More Accurate Prediction of Activation Energies for Polyalcohol Dehydrogenation on Transition Metal Catalysts in Water. *Catal. Sci. Technol.* **2016**, *6* (17), 6615−6624.
(50) Valter, M.; Dos Santos, E. C.; Pettersson, L. G. M.; Hellman, A. Selectivity of the First Two Glycerol Dehydrogenation Steps Determined Using Scaling Relationships. *ACS Catal.* **2021**, *11* (6), 3487−3497.
(51) Feng, S.; Takahashi, K.; Miura, H.; Shishido, T. One-Pot Synthesis of Lactic Acid from Glycerol over a Pt/L-Nb2O5 Catalyst under Base-Free Conditions. *Fuel Process. Technol.* **2020**, *197* (2020), 106202.